Ionics
DOI 10.1007/s11581-015-1631-8

ORIGINAL PAPER

Glycerol oxidation reaction using PdAu/C electrocatalysts

Cristiane Angélica Ottoni[1] · **Sirlane G. da Silva**[2] · **Rodrigo F. B. De Souza**[2] · **Almir Oliveira Neto**[2]

Received: 8 October 2015 / Revised: 1 December 2015 / Accepted: 29 December 2015

Abstract Glycerol oxidation reactions were evaluated using PdAu/C electrocatalysts under alkaline conditions. These electrocatalysts were synthesized in different ratios (100:0, 75:25, 50:50, 25:75, and 0:100), using the borohydride reduction method. The materials were characterized with X-ray diffraction (XRD), transmission electron microscopy (TEM), and electrochemical techniques associated by in situ attenuated total reflectance Fourier transformed infrared spectroscopy (ATR-FTIR). According to the XRD diffractograms, the presence of Pd and Au (face-centered cubic (fcc)) phases and Pd-Au (fcc) alloys were detected. Cyclic voltammetry assisted by ATR-FTIR in situ and chronoamperometry experiments revealed that the addition of Au remarkably enhances the electrocatalytic activity, due to the action of bifunctional effect, with addition of the interactions of alcohoxide with hydroxylate species in gold surface, and the stability of Pd/C catalysts. Highest current density (≈4 mA mg_{metal}^{-1}) was achieved for the catalyst $Pd_{50}Au_{50}$/C and $Pd_{75}Au_{25}$/C, which is two times higher than that achieved by Pd/C (2 mA mg_{metal}^{-1}), demonstrating the beneficial effect of the PdAu alloy.

Keywords PdAu alloy · Palladium-electrocatalyst · Glycerol oxidation reaction

✉ Cristiane Angélica Ottoni
aolivei@ipen.br

[1] Biosciences Institute, São Paulo State University - UNESP, Coastal Campus, 11330-900 São Vicente, Brazil

[2] Instituto de Pesquisas Energéticas e Nucleares, IPEN/CNEN-SP, Av. Prof. Lineu Prestes, 2242 Cidade Universitária, CEP 05508-900, São Paulo, SP, Brazil

Introduction

Recently, glycerol oxidation reaction (GOR) studies have been receiving increased attention due to their potential use for producing higher-valued oxygenated chemicals, including glyceric acid, tartronic acid, and other compounds [1–4]. Furthermore, energy involved during the product formation can, theoretically, be used as electrical energy and be applied in fuel cells, where the complete oxidation of alcohols to CO_2 occurs. These were the hypotheses that led to the increase of research on catalysts. In this context, direct alkaline alcohol fuel cells (DAAFCs) represent one of the most promising approaches for renewable and clean energy devices [5, 6].

Glycerol has been the preferred alternative to fuels when using DAAFCs, due to a wide range of characteristics. This compound is a non-flammable, non-volatile liquid (boiling point 290 °C). It is electrochemically oxidizable, providing up to 14 F mol^{-1} when fully oxidized, and displays relatively high theoretical energy density (5.0 kWh kg^{-1}). Furthermore, glycerol can be obtained from methanolysis of vegetable oils and thus be produced in renewable and environmentally friendly ways [5–7]. However, glycerol has three functional groups and a large number of products can be formed from its oxidation, which is one of the key problems when designing a catalyst and determining the operating conditions for the selective formation of a product or to optimize the generation of electric power [7, 8].

Within the catalysts use for GOR, those based on platinum (Pt) have demonstrated acceptable power densities [2, 9, 10]. This is the main reason why many researchers have been devoted to modify Pt-based catalysts to obtain more activity, with higher selectivity at cheaper costs [10]. Other optimization efforts focus on designing new Pt-free catalysts for oxidation of alcohols in alkaline medium. One example of this is the use of palladium (Pd), which is a good catalyst for the

Published online: 21 January 2016

oxidation of primary and secondary alcohols in alkaline solutions [2, 8, 9] and has the advantages of being more available in nature and cheaper than Pt.

Pd-based catalysts are more active for the oxidation of alcohols in alkaline media than Pd alone. There are many descriptions of different approaches of binary and ternary materials for alcohol oxidation such as the following: PdSn [11, 12], PdNi [12, 13], PdAu [2, 14, 15], and others [16–18]. Another metal that has been studied for the same purposes is gold (Au), which has been reported to be active towards oxidation reactions in alkaline medium, due to its ability of hydroxylating its surface that interacts strongly with alcohoxide and simultaneously achieves higher stability than other materials like Pt and Pd [15, 19].

In the present work, Pd, PdAu, and Au carbon-supported electrocatalysts have been synthesized through the borohydride reduction method. Their crystal phase and morphology was determined by X-ray diffraction (XRD) and transmission electron microscopy (TEM). The catalytic activity of these catalysts towards glycerol oxidation was studied by comparing some of the critical kinetic parameters evaluated through several electrochemical techniques like cyclic voltammetry (CV), in situ attenuated total reflectance Fourier transform infrared spectroscopy (ATR-FTIR), and chronoamperometry.

Material and methods

Pd/C, Au/C, and PdAu/C electrocatalysts (20 % of metal loading) were prepared using the sodium borohydride method [14, 20, 21] with different Pd:Au atomic ratios (100:0, 75:25, 50:50, 25:75, and 0:100) using $H_2PtCl_6.6H_2O$ (Aldrich) and $HAuCl_4.3H_2O$ (Aldrich). The process of metal reduction started when the metal sources were added and diluted in a mixture of water/2-propanol (50/50, *v*/*v*) followed by addition of carbon Vulcan XC 72 support dispersed in the solution. The mixture was submitted to an ultrasonic bath for 10 min. A solution prepared with excess of $NaBH_4$ (Aldrich) and 0.1 mol L^{-1} NaOH was added to the mixture and kept for 30 min under stirring at room temperature. After this procedure, the final mixture was filtered and the resultant product washed with 2 L of distilled water and dried at 70 °C for 2 h.

TEM was carried out using a JEOL JEM-2100 electron microscope operated at 200 kV. The particle distribution histogram was determined by measuring 150 particles per micrograph. XRD analyses were carried out in a Miniflex II model Rigaku diffractometer using CuKα ($\lambda = 1.54056$ Å). The diffractograms were recorded at 2θ in the range 20–90°, with step size of 0.05° and scan time of 2 s per step.

Electrochemical studies of the electrocatalysts were carried out using an electrochemical cell with three electrodes. The working electrodes were prepared by thin porous coating technique [14, 22], where 20 mg of the electrocatalyst was added to a solution containing 50 mL of water and 100 μL of a 6 % polytetrafluoroethylene (PTFE) suspension. The resulting mixture was treated in an ultrasound bath for 10 min, filtered, and deposited on the working electrode (0.36 cm^2 area and 0.30 mm deep). The reference electrode was an Ag/AgCl (3 mol L^{-1} KCl) and the counter electrode was a Pt plate. Electrochemical measurements were made using a potentiostat-galvanostat Autolab 302N. CV was performed using 1.0 mol L^{-1} glycerol in 1.0 mol L^{-1} KOH solution saturated with N_2. Chronoamperometry experiments were performed using 1.0 mol L^{-1} glycerol in 1.0 mol L^{-1} KOH solution, at −0.35 V, at room temperature. The currents in cyclic voltammograms and chronoamperograms were normalized per gram of metal.

The spectro-electrochemical in situ ATR-FTIR measurements were performed with a Nicolet 6700 FTIR spectrometer, equipped with a MCT detector cooled with liquid N_2, ATR accessory (MIRacle with a Diamond/ZnSe Crystal Plate PIKE®) and an electrochemical cell as described in the literature [14, 23–25]. The working electrodes were the same used for the electrochemical experiments in the presence of 1.0 mol L^{-1} glycerol with 1 mol L^{-1} KOH. The absorbance spectra were collected as the ratio R:R_0, where R represents a spectrum at a given potential and R_0 is the spectrum collected at −0.85 V. Positive and negative directional bands represent gain and loss of species at the sampling potential, respectively. The spectra were computed from 96 interferograms, averaged from 3000 to 850 cm^{-1}, with the spectral resolution set to 8 cm^{-1}. Initially, a reference spectrum (R_0) was measured at −0.85 V, and the sample spectra were collected after applying successive potential steps from 0.1 to 0.05 V.

Results and discussion

TEM images of the Pd/C, PdAu/C, and Au/C materials were obtained (Fig. 1). As can be observed, all electrocatalysts are well dispersed with some agglomerations on the carbon powder. The mean particle sizes are as follows: 6.1, 4.3, 5.2, 6.1, and 9.2 nm for Pd, $Pd_{75}Au_{25}$, $Pd_{50}Au_{50}$, $Pd_{25}Au_{75}$, and Au respectively. For these Pd-based materials, it is possible to observe a decrease in the average particle size when gold was added. However, when the amount of gold was increased in the composition, the average particle size increased again probably due to a capacity of agglomeration of gold atoms during the reduction process. It is also interesting to note that the gold nanoparticles are at least 50 % bigger than those containing Pd, fact analogous to other similar materials reported in the literature [13, 26].

The XRD patterns of Pd/C, PdAu/C, and Au/C catalysts were collected in the range of 20° to 90° and are shown in Fig. 2a. All of them displayed a typical face-centered cubic (fcc) pattern for Pd and Au [6, 10, 21], with the diffraction

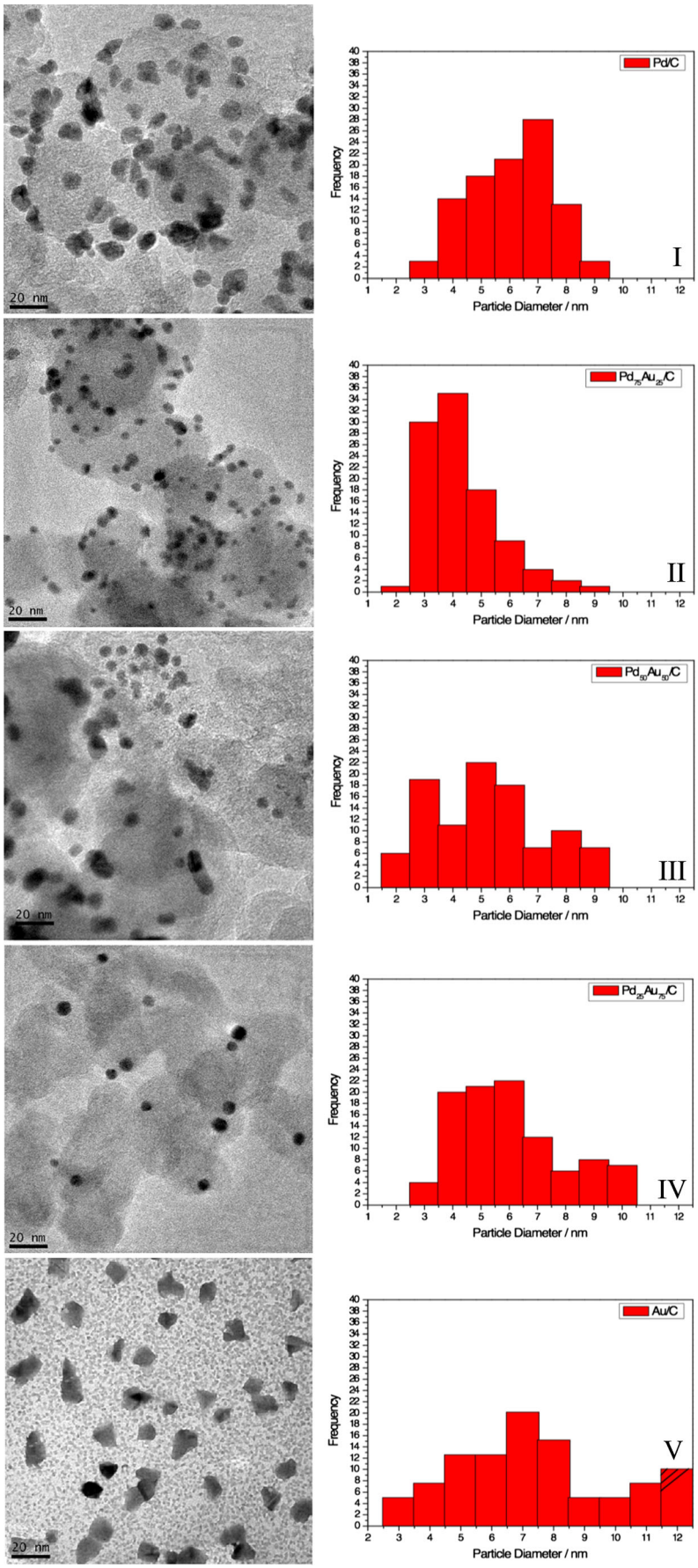

Fig. 1 TEM images and corresponding histograms of the (I) Pd/C, (II) PdAu/C 75:25, (III) PdAu/C 50:50, (IV) PdAu/C 25:75, and (V) Au/C nanomaterials

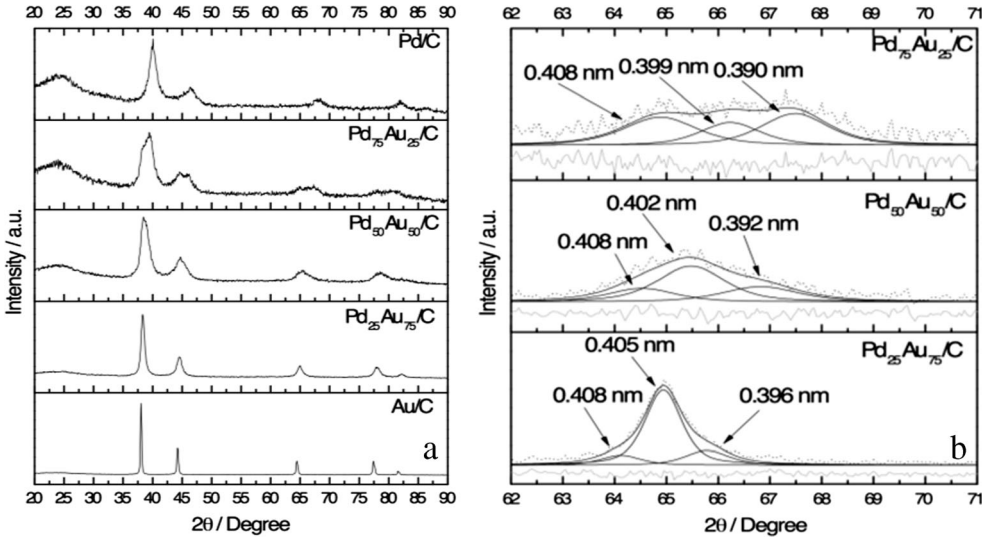

Fig. 2 **a** XRD patterns of Pd/C, PdAu/C, and Au/C catalysts. **b** Pawley refinement of peak (220) for PdAu/C materials with *dot line* for experimental measure, *black lines* for modeled, and *grey line* for residual line

peaks at ~39°, ~46°, ~66°, and ~80° assigned to the corresponding (111), (200), (220), and (311), respectively. The peak around 25° present for all the catalysts refers to the graphite (002) on the face of the carbon support [27, 28]. For the binary composite catalysts of PdAu (75:25, 50:50, and 25:75), it is possible to see a deformation of the peaks related to the noble metals and its shift 2θ values between the Pd and Au. To obtain more information about this shift, the XRD pattern was refined using the Pawley method with the Fityk 0.98 software [29, 30]. In Fig. 2b, it is possible to observe the changes in the peak shape as a result of the contribution of Pd (fcc) ($a = 0.390$ nm) (JCPDS 05-0682), Au (fcc) ($a = 0.408$ nm) (JCPDS 04-0784), and different non-stoichiometric PdAu alloy degree ($a = 0.392$ until $a = 0.405$ nm) phases. This intermediate lattice values can indicate the transition of gold atoms inserted into the palladium crystalline network of palladium atoms or inserted in gold crystalline network, following the variation of these metals in the catalyst composition. Furthermore, the Pd peak in $Pd_{25}Au_{75}/C$ material was not detected.

The cyclic voltammograms of the Pd- and Au-based catalysts (Fig. 3) show the hydrogen adsorption-desorption region on Pd (−0.85 and −0.50 V vs. Ag/AgCl) which is well defined for Pd/C. This definition as well as the intensity decreases with the decreasing load of Pd, and it even disappears in the material $Pd_{25}Au_{75}/C$, probably because there is less phase of only Pd as observed in XRD. In the reverse sweep, there is a pronounced peak between −0.1 and −0.6 V attributed to the reduction of Pd oxide [15]. The potential of the center of this peak is different for each material, resulting from the amount of surface Pd oxides and by the influence of added gold [13].

Figure 4 shows the profiles obtained by the linear sweep voltammetry experiments for GOR on Pd and Au materials. We noticed that all the materials have a close onset potential for glycerol oxidation (−0.48 V ± 20 mV). On these profiles, it is also possible to observe a peak at approximately −0.69 V, and when compared with the cyclic voltammetry of Fig. 3, we can conclude that this is not linked with hydrogen desorption region because this peak is present on the gold catalyst but no

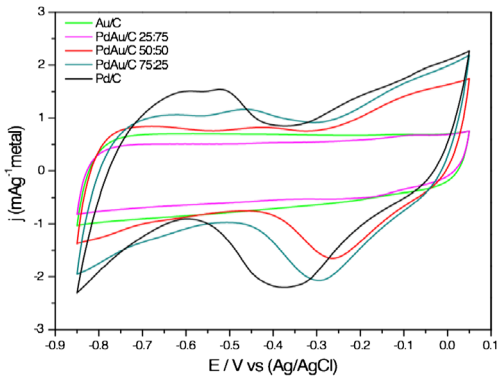

Fig. 3 Cyclic voltammograms of Pd/C, PdAu/C, and Au/C catalysts in KOH 1.0 mol L^{-1} aqueous solution ($v = 10$ mV s^{-1}) at room temperature

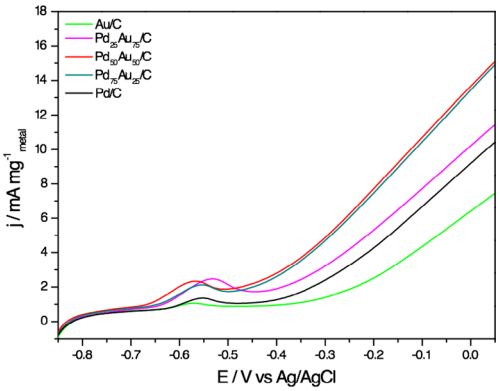

Fig. 4 Linear sweep voltammograms for GOR on Pd/C, Au/C, and PdAu/C catalysts in KOH 1.0 mol L^{-1} and glycerol 1.0 mol L^{-1}, $v = 10$ mV s^{-1}

peaks were observed for hydrogen desorption, leading us to conclude that it possibly corresponds to any oxidative process that will be indicated in the in situ ATR-FTIR spectra (Fig. 5).

In order to correlate the activity of glycerol oxidation with the preferential pathway, we also use the in situ ATR-FTIR (Fig. 5). For these spectra, we observed a decrease of the glycerol bands (1004, 1041, and 1094 cm^{-1}) [31, 32] with

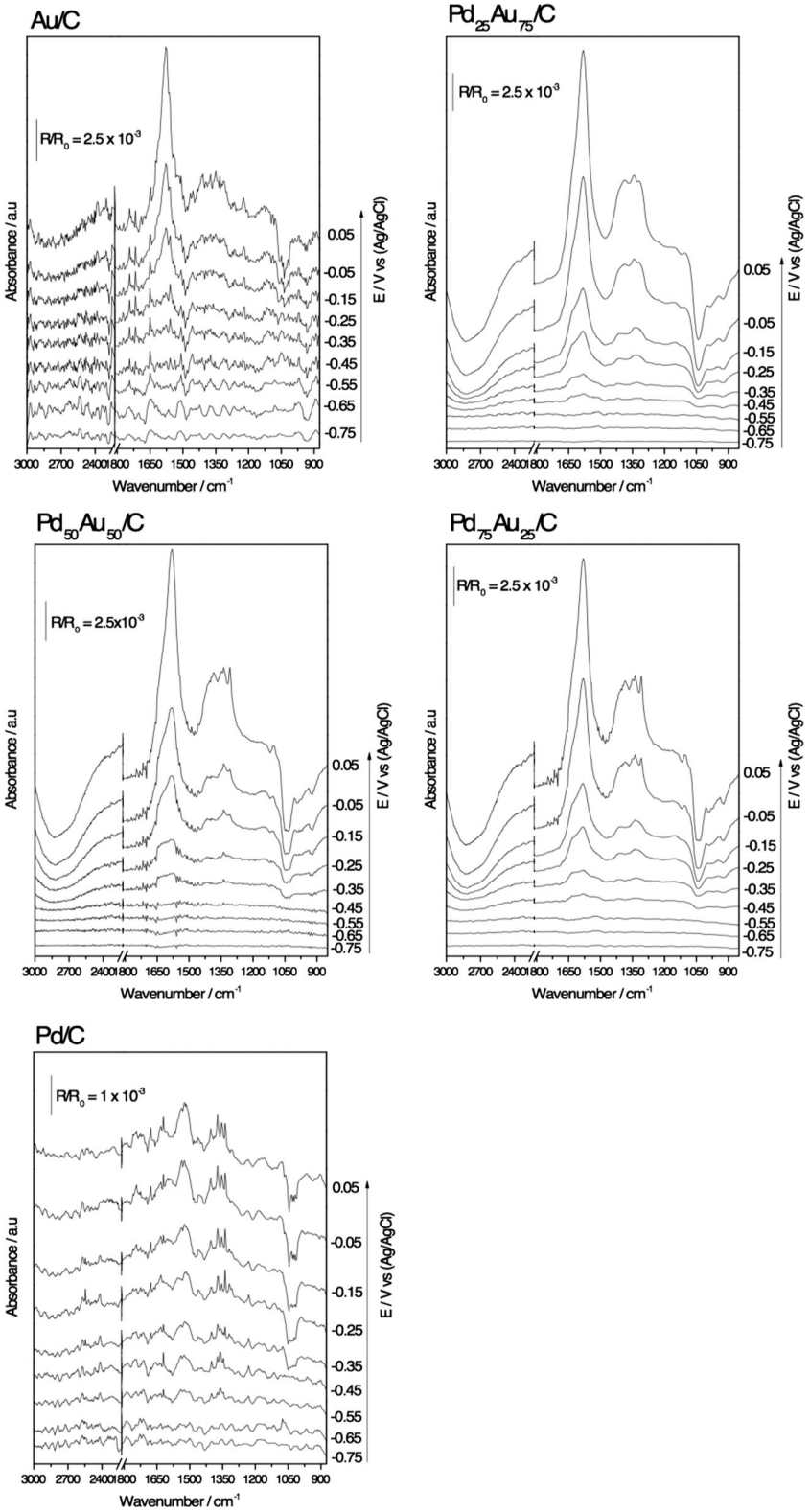

Fig. 5 In situ ATR-FTIR taken at −0.75 to 0.05 V using Pd/C, PdAu/C, and Au/C in KOH 1.0 mol L^{-1} with glycerol 1.0 mol L^{-1}. The backgrounds were collected at −0.85 V

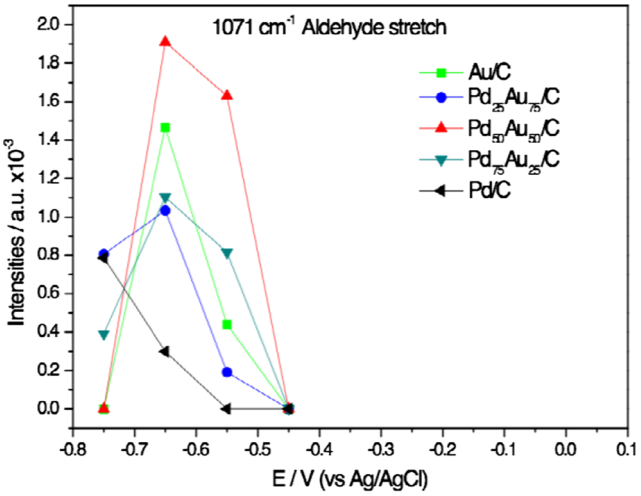

Fig. 6 Glyceraldehyde (aldehyde stretch) integrated intensities bands as a function of the potential. Data extracted from Fig. 5

an increase of the potential indicating glycerol consumption. We also noticed an increase of the bands resulting from 1071 cm^{-1} corresponding to glyceraldehyde [19], 1225 cm^{-1} to formate [10], 1335 cm^{-1} to 1,3-dihydroxy-2-propanone [13], 1345 cm^{-1} to tortronate [33], 1355 cm^{-1} to hydroxypyruvate [31, 32], 1377 cm^{-1} to glycerate [13, 34, 35], ~1405 cm^{-1} to carbonate [31], ~1589 cm^{-1} to H–O–H deformation, symmetric COO^{-} stretch to glycolate and glyoxylate [31], ~1665 cm^{-1} to carbonyl and carboxyl stretches [31, 34], and 1723 cm^{-1} to carboxyl stretching [31, 36], and CO_2 signal (2343 cm^{-1}) [37] was not detected in these spectra.

In order to evaluate the catalyst composition effect in the products with the application of different potentials, all bands were deconvoluted to Lorentzian line forms [23]. Figure 6 shows the integrated intensities of aldehyde stretch corresponding to glyceraldehyde (1071 cm^{-1}) detected in the first potential values. However, these bands disappear very quickly which can be due to low stability of the primary aldehydes under alkaline condition [19] or to the glycerol consumption band interference with the detection of the glyceraldehyde band. The production and consumption of the glyceraldehyde band can be explained by the peak at 0.69 V, observed in linear sweep voltammograms (Fig. 4).

Figure 7 shows the integrated intensities of the bands for glycerate (1377 cm^{-1}) and tartronate (1345 cm^{-1}). Literature suggests that glycerate is the precursor of tartronate [13, 35], and the results obtained for Pd/C, PdAu/C, and Au/C confirm that this is true in electrochemical cells with three electrodes, caused initially by the production of glycerate and later by the production of tartronate. Furthermore, it is possible to observe that for PdAu/C materials, the intensity of the tartronate bands is higher than those measured for the Pd/C and Au/C catalysts, probably due to synergistic effects provided by the Pd and Au. Pd acts as an adsorption site [2, 4, 15] and Au interacts with oxygenated species [19] favoring the production of more oxidized products. Additionally, it is possible to notice that materials containing gold shift from the onset potential to produce carboxylic acids that are 100 mV less negative than just Pd/C.

Figure 8 shows the integration of bands corresponding to 1, 3-dihydroxy-2-propanone and hydroxypyruvate, where it is possible to observe that the intensities of these species are higher for PdAu materials than the ones obtained for Pd/C and Au/C. It is interesting to note that for Pd/C 1,3-dihydroxy-2-propanone, onset potential is 100 mV less negative than for hydroxypyrivate, which is in agreement with what has been reported in the literature [9, 13] that states that 1,3-dihydroxy-2-propanone is an oxidation product from hydroxypyruvate. This is an indication that the presence of gold can produce the hydroxypyruvate by a parallel pathway.

Figure 9 shows the integration bands of glycerol oxidation products that require C–C bond break (glycolate, oxalate, formate, and carbonate). It is possible to see that Pd/C and $Pd_{75}Au_{25}$/C have oxalate and glycolate production onset with

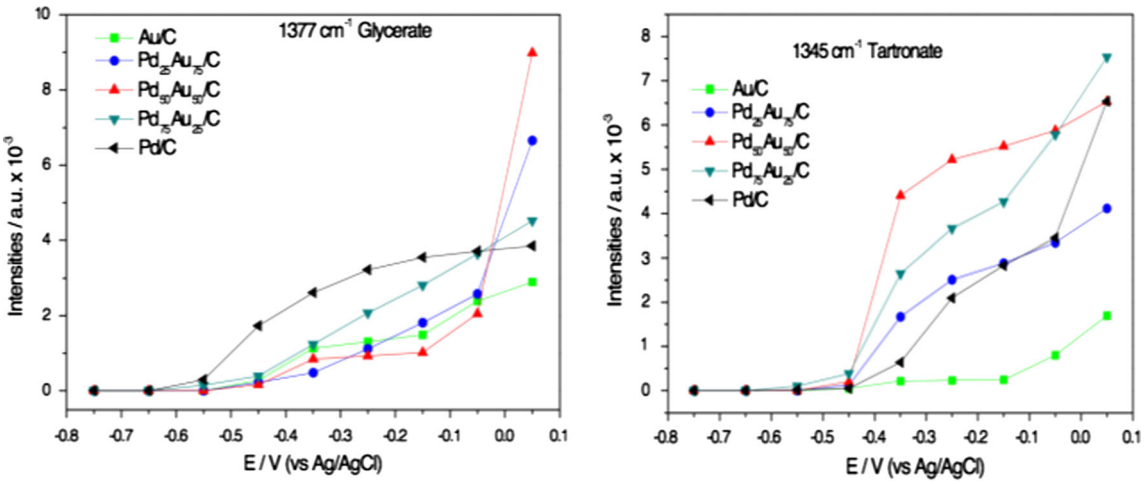

Fig. 7 Glycerate- and tartronate-integrated intensity bands as a function of the potential. Data extracted from Fig. 5

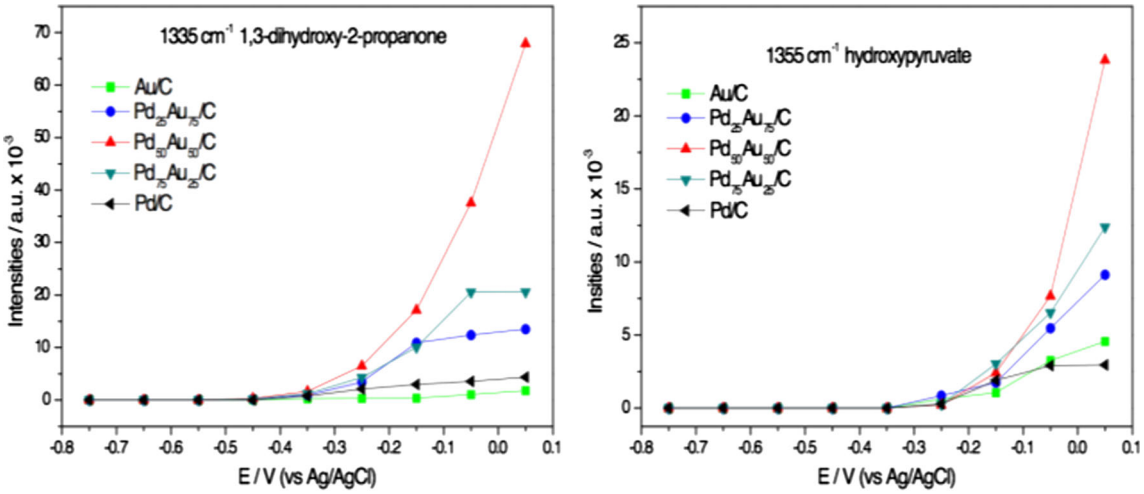

Fig. 8 1,3-Dihydroxy-2-propanone- and hydroxypyruvate-integrated intensity bands as a function of the potential. Data extracted from Fig. 5

more negative potential than other materials. In addition, it is also possible to note that near −0.05 V, the band relative to glycolate is extinct, and the oxalate band is increased in the same potential range. These materials also have the more negative onset potential and higher intensities for carbonate ion than others catalysts. For $Pd_{50}Au_{50}/C$ catalyst, no glycolate and oxalate bands were detected. Nevertheless, this catalyst produces formate and carbonate, indicating that the

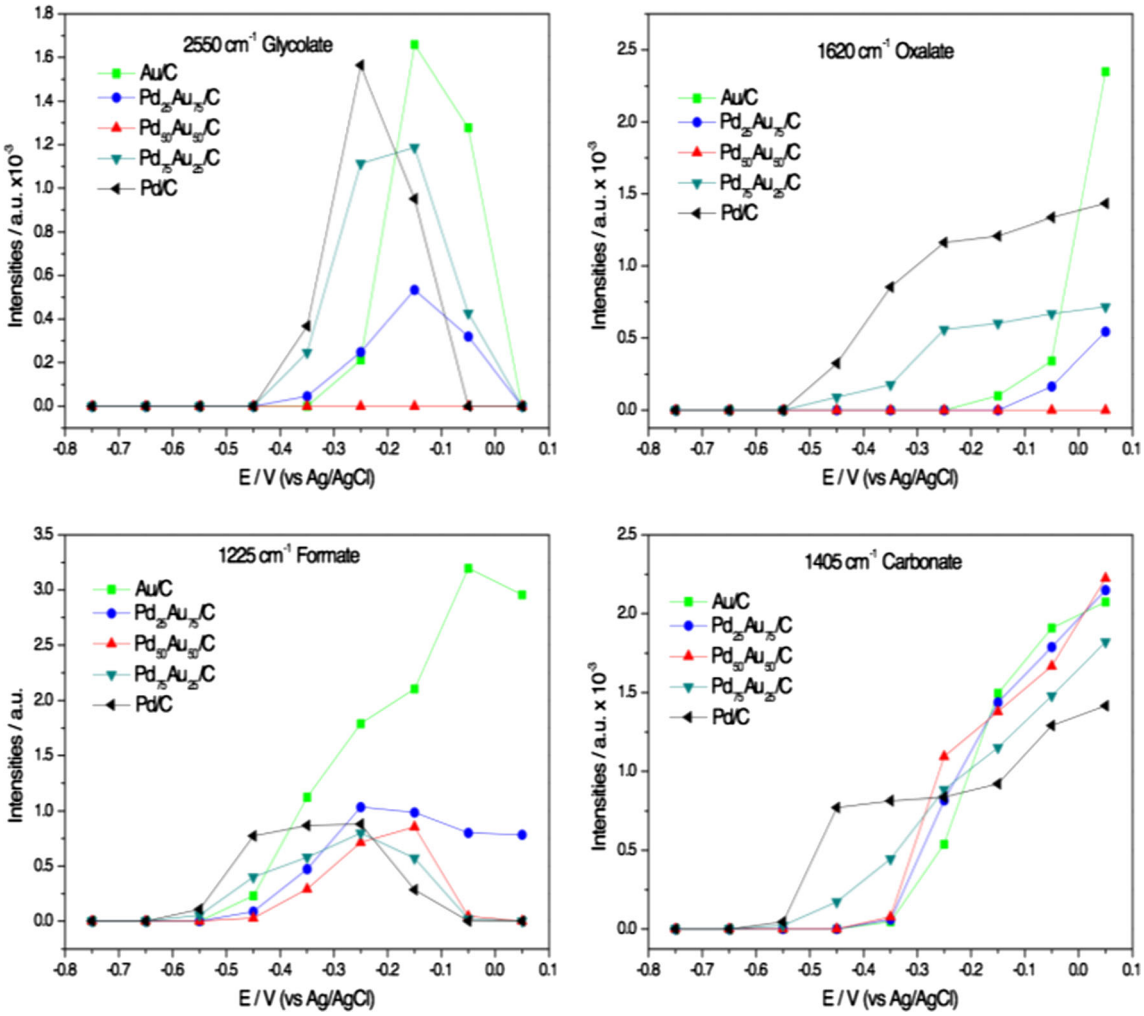

Fig. 9 Glycolate-, oxalate-, formate-, and carbonate-integrated intensity bands as a function of the potential. Data extracted from Fig. 5

phases present in $Pd_{50}Au_{50}$/C alloy can break all the C–C bonds of glycerol in a single process.

Formate bands are produced for all materials and will be fully extinguished until −0.05 V, except for Au/C and $Pd_{25}Au_{75}$/C that contain this species at 0.05 V, indicating that formate is consumed faster in materials that exhibit a Pd phase. Au/C and $Pd_{25}Au_{75}$/C catalysts present less negative onset potential for glycolate production, and these bands disappear at 0.05 V. This extinction coincides with an increase in intensity of the oxalate band.

Figure 10 shows current-time curves obtained during glycerol electro-oxidation 1 mol L^{-1} in KOH 1 mol L^{-1}. The measured current density for glycerol oxidation at −0.35 V can be observed for all the cases where there is a strong current decay in the first minutes, followed by a slow decay until 4.3 mA mg^{-1} ($Pd_{50}Au_{50}$/C) > 4.0 mA mg^{-1} ($Pd_{75}Au_{25}$/C) > ~2.5 mA mg^{-1} (Pd and $Pd_{25}Au_{75}$/C) > 1.4 mA mg^{-1} (Au/C).

The higher activity of $Pd_{50}Au_{50}$/C electrocatalyst, when compared to other materials, is probably a result from the occurrence of alloy phases present in this composition and from the preference for the pathway of production of carboxylic acids which is more oxidized and has easier capability of breaking all C–C bonds of glycerol in just one step.

Conclusion

In summary, we found that PdAu/C is more active than Pd/C and Au/C. In all compositions of Pd:Au, alloys were formed. The onset potential determined for GOR is close to −0.48 V for all electrocatalysts, whereas PdAu containing materials are more active than the separated noble metals. We hypothesize that this is due to the synergistic effect of PdAu alloy, the Pd adsorption capacity, and the Au interaction with oxygen species. Most importantly, the PdAu (50:50) composition was found to be the most active, owing to its preference for producing more oxidized carboxylic acids and for its greater facility in breaking all C–C bonds of glycerol in one step.

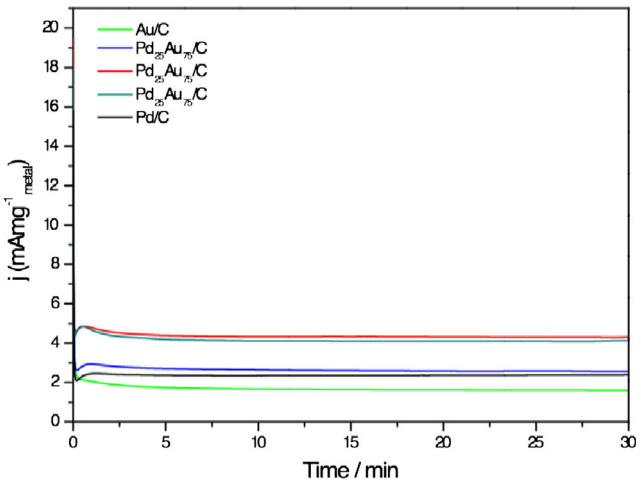

Fig. 10 Current-time curves at −0.35 V for Pd/C, Au/C, and PdAu/C electrocatalysts, in 1.0 mol L^{-1} glycerol in 1.0 mol L^{-1} KOH

Acknowledgments The authors thank CNPq (150111/2015-0), FAPESP (2014/09087-4) and CAPES for the financial support and CCTM from IPEN/CNEN-SP for the TEM measurements.

References

1. Rodriguez AA, Williams CT, Monnier JR (2014) Selective liquid-phase oxidation of glycerol over Au–Pd/C bimetallic catalysts prepared by electroless deposition. Appl Catal A 475:161–168. doi:10.1016/j.apcata.2014.01.011
2. Lam BTX, Chiku M, Higuchi E, Inoue H (2015) Preparation of PdAg and PdAu nanoparticle-loaded carbon black catalysts and their electrocatalytic activity for the glycerol oxidation reaction in alkaline medium. J Power Sources 297:149–157. doi:10.1016/j.jpowsour.2015.07.086
3. Han X, Chadderdon DJ, Qi J, Xin L, Li W, Zhou W (2014) Numerical analysis of anion-exchange membrane direct glycerol fuel cells under steady state and dynamic operations. Int J Hydrogen Energy 39(34):19767–19779. doi:10.1016/j.ijhydene.2014.08.144
4. Zhang Z, Xin L, Li W (2012) Electrocatalytic oxidation of glycerol on Pt/C in anion-exchange membrane fuel cell: cogeneration of electricity and valuable chemicals. Appl Catal B 119–120:40–48. doi:10.1016/j.apcatb.2012.02.009
5. Fashedemi OO, Ozoemena KI (2014) Comparative electrocatalytic oxidation of ethanol, ethylene glycol and glycerol in alkaline medium at Pd-decorated FeCo@Fe/C core-shell nanocatalysts. Electrochim Acta 128:279–286. doi:10.1016/j.electacta.2013.10.194
6. Zhang Z, Xin L, Qi J, Chadderdon DJ, Li W (2013) Supported Pt, Pd and Au nanoparticle anode catalysts for anion-exchange membrane fuel cells with glycerol and crude glycerol fuels. Appl Catal B 136–137:29–39. doi:10.1016/j.apcatb.2013.01.045
7. Fernández PS, Martins ME, Camara GA (2012) New insights about the electro-oxidation of glycerol on platinum nanoparticles supported on multi-walled carbon nanotubes. Electrochim Acta 66:180–187
8. Ferreira RS Jr, Janete Giz M, Camara GA (2013) Influence of the local pH on the electrooxidation of glycerol on palladium–rhodium electrodeposits. J Electroanal Chem 697:15–20. doi:10.1016/j.jelechem.2013.03.007
9. Rostami H, Omrani A, Rostami AA (2015) On the role of electrodeposited nanostructured Pd–Co alloy on Au for the electrocatalytic oxidation of glycerol in alkaline media. Int J Hydrogen Energy 40(30):9444–9451. doi:10.1016/j.ijhydene.2015.05.154
10. Ottoni CA, da Silva SG, De Souza RFB, Neto AO (2015) PtAu electrocatalyst for glycerol oxidation reaction using a ATR-FTIR/single direct alkaline glycerol/air cell in situ study. Electrocatalysis. doi:10.1007/s12678-12015-10277-12677
11. Mao H, Wang L, Zhu P, Xu Q, Li Q (2014) Carbon-supported PdSn–SnO2 catalyst for ethanol electro-oxidation in alkaline media. Int J Hydrogen Energy 39(31):17583–17588. doi:10.1016/j.ijhydene.2014.08.079
12. Ramulifho T, Ozoemena KI, Modibedi RM, Jafta CJ, Mathe MK (2013) Electrocatalytic oxidation of ethylene glycol at palladium-bimetallic nanocatalysts (PdSn and PdNi) supported on sulfonate-functionalised multi-walled carbon nanotubes. J Electroanal Chem 692:26–30. doi:10.1016/j.jelechem.2012.12.010

13. Simões M, Baranton S, Coutanceau C (2010) Electro-oxidation of glycerol at Pd based nano-catalysts for an application in alkaline fuel cells for chemicals and energy cogeneration. Appl Catal B 93 (3–4):354–362. doi:10.1016/j.apcatb.2009.10.008
14. Fontes EH, Piasentin RM, Ayoub JMS, da Silva JCM, Assumpção MHMT, Spinacé EV, Neto AO, de Souza RFB (2015) Electrochemical and in situ ATR-FTIR studies of ethanol electro-oxidation in alkaline medium using PtRh/C electrocatalysts. Mater Renew Sustain Energy 4(1):1–10. doi:10.1007/s40243-015-0043-z
15. Xu JB, Zhao TS, Shen SY, Li YS (2010) Stabilization of the palladium electrocatalyst with alloyed gold for ethanol oxidation. Int J Hydrogen Energy 35(13):6490–6500. doi:10.1016/j.ijhydene.2010.04.016
16. Munoz F, Hua C, Kwong T, Tran L, Nguyen TQ, Haan JL (2015) Palladium-copper electrocatalyst for the promotion of the electrochemical oxidation of polyalcohol fuels in the alkaline direct alcohol fuel cell. Appl Catal B 174:323–328. doi:10.1016/j.apcatb.2015.03.027
17. Shen SY, Zhao TS, Xu JB (2010) Carbon-supported bimetallic PdIr catalysts for ethanol oxidation in alkaline media. Electrochim Acta 55(28):9179–9184. doi:10.1016/j.electacta.2010.09.018
18. Brandalise M, Tusi MM, Piasentin RM, Santos MCD, Spinacé EV, Neto AO (2012) Synthesis of PdAu/C and PdAuBi/C electrocatalysts by borohydride reduction method for ethylene glycol electro-oxidation in alkaline medium. Int J Electrochem Sci 7 (10):9609–9621
19. Kwon Y, Lai SCS, Rodriguez P, Koper MTM (2011) Electrocatalytic oxidation of alcohols on gold in alkaline media: base or gold catalysis? J Am Chem Soc 133(18):6914–6917. doi:10.1021/ja200976j
20. Nandenha J, De Souza RFB, Assumpcao MHMT, Spinace EV, Neto AO (2013) Preparation of PdAu/C-Sb2O5 center dot SnO2 electrocatalysts by borohydride reduction process for direct formic acid fuel cell. Ionics 19(9):1207–1213. doi:10.1007/s11581-013-0955-5
21. Neto AO, Nandenha J, De Souza RFB, Buzzo GS, Silva JCM, Spinacé EV, Assumpção MHMT (2014) Anodic oxidation of formic acid on PdAuIr/C-$Sb_2O_5 \cdot SnO_2$ electrocatalysts prepared by borohydride reduction. J Fuel Chem Technol 42(7):851–857. doi:10.1016/S1872-5813(14)60037-2
22. Neto AO, Brandalise M, Dias RR, Ayoub JMS, Silva AC, Penteado JC, Linardi M, Spinacé EV (2010) The performance of Pt nanoparticles supported on Sb2O5.SnO2, on carbon and on physical mixtures of Sb2O5.SnO2 and carbon for ethanol electro-oxidation. Int J Hydrogen Energy 35(17):9177–9181. doi:10.1016/j.ijhydene.2010.06.028
23. Silva JCM, Parreira LS, De Souza RFB, Calegaro ML, Spinacé EV, Neto AO, Santos MC (2011) PtSn/C alloyed and non-alloyed materials: differences in the ethanol electro-oxidation reaction pathways. Appl Catal B 110:141–147
24. De Souza RFB, Silva JCM, Simoes FC, Calegaro ML, Neto AO, Santos MC (2012) New approaches for the ethanol oxidation reaction of Pt/C on carbon cloth using ATR-FTIR. Int J Electrochem Sci 7(6):5356–5366
25. Henrique RS, De Souza RFB, Silva JCM, Ayoub JMS, Piasentin RM, Linardi M, Spinacé EV, Santos MC, Neto AO (2012) Preparation of Pt/C-In 2O 3.SnO 2 electrocatalysts by borohydride reduction process for ethanol electro-oxidation. Int J Electrochem Sci 7(3):2036–2046
26. Ketchie WC, Fang Y-L, Wong MS, Murayama M, Davis RJ (2007) Influence of gold particle size on the aqueous-phase oxidation of carbon monoxide and glycerol. J Catal 250(1):94–101. doi:10.1016/j.jcat.2007.06.001
27. Modibedi RM, Masombuka T, Mathe MK (2011) Carbon supported Pd–Sn and Pd–Ru–Sn nanocatalysts for ethanol electro-oxidation in alkaline medium. Int J Hydrogen Energy 36(8):4664–4672. doi:10.1016/j.ijhydene.2011.01.028
28. Wang H, Liu Z, Ji S, Wang K, Zhou T, Wang R (2013) Ethanol oxidation activity and structure of carbon-supported Pt-modified PdSn-SnO2 influenced by different stabilizers. Electrochim Acta 108:833–840
29. Pawley GS (1981) Unit-cell refinement from powder diffractions scans. J Appl Crystallogr 14:357–361. doi:10.1107/s0021889881009618
30. Wojdyr M (2010) Fityk: a general-purpose peak fitting program. J Appl Crystallogr 43:1126–1128. doi:10.1107/s0021889810030499
31. Falase A, Main M, Garcia K, Serov A, Lau C, Atanassov P (2012) Electrooxidation of ethylene glycol and glycerol by platinum-based binary and ternary nano-structured catalysts. Electrochim Acta 66:295–301. doi:10.1016/j.electacta.2012.01.096
32. Jeffery DZ, Camara GA (2010) The formation of carbon dioxide during glycerol electrooxidation in alkaline media: first spectroscopic evidences. Electrochem Commun 12(8):1129–1132. doi:10.1016/j.elecom.2010.06.001
33. Cai J, Ma H, Zhang J, Du Z, Huang Y, Gao J, Xu J (2014) Catalytic oxidation of glycerol to tartronic acid over Au/HY catalyst under mild conditions. Chin J Catal 35(10):1653–1660. doi:10.1016/S1872-2067(14)60132-7
34. Schnaidt J, Heinen M, Denot D, Jusys Z, Jürgen Behm R (2011) Electrooxidation of glycerol studied by combined in situ IR spectroscopy and online mass spectrometry under continuous flow conditions. J Electroanal Chem 661(1):250–264. doi:10.1016/j.jelechem.2011.08.011
35. Simões M, Baranton S, Coutanceau C (2011) Enhancement of catalytic properties for glycerol electrooxidation on Pt and Pd nanoparticles induced by Bi surface modification. Appl Catal B 110:40–49. doi:10.1016/j.apcatb.2011.08.020
36. Martins CA, Giz MJ, Camara GA (2011) Generation of carbon dioxide from glycerol: evidences of massive production on polycrystalline platinum. Electrochim Acta 56(12):4549–4553. doi:10.1016/j.electacta.2011.02.076
37. Neto AO, Nandenha J, Assumpção MHMT, Linardi M, Spinacé EV, de Souza RFB (2013) In situ spectroscopy studies of ethanol oxidation reaction using a single fuel cell/ATR-FTIR setup. Int J Hydrogen Energy 38(25):10585–10591. doi:10.1016/j.ijhydene.2013.06.026